Available online at www.sciencedirect.com
SCIENCE DIRECT
Journal of Solid State Chemistry 179 (2006) 2707–2713
JOURNAL OF SOLID STATE CHEMISTRY
www.elsevier.com/locate/jssc

Crystal structure, electronic structure and physical properties of the new low-valent thallium silicon telluride $Tl_6Si_2Te_6$ in comparison to $Tl_6Ge_2Te_6$

Abdeljalil Assoud, Navid Soheilnia, Holger Kleinke*

Department of Chemistry, University of Waterloo, Waterloo, Ont., Canada N2L 3G1

Received 15 March 2006; received in revised form 17 May 2006; accepted 28 May 2006
Available online 3 June 2006

Abstract

The title compounds were prepared from the elements in the stoichiometric ratio at 800 °C under exclusion of air. $Tl_6Si_2Te_6$ crystallizes in the space group $P\bar{1}$, isostructural with $Tl_6Ge_2Te_6$, with $a = 9.4235(6)$ Å, $b = 9.6606(7)$ Å, $c = 10.3889(7)$ Å, $\alpha = 89.158(2)°$, $\beta = 96.544(2)°$, $\gamma = 100.685(2)°$, $V = 923.3(1)$ Å^3 ($Z = 2$). Its structure is composed of dimeric $[Si_2Te_6]^{6-}$ units with a Si–Si single bond, while the Tl atoms are irregularly coordinated by five to six Te atoms. Numerous weakly bonding Tl–Tl contacts exist. Both title compounds are black semiconductors with small band gaps, calculated to be 0.9 eV for $Tl_6Si_2Te_6$ and 0.5 eV for $Tl_6Ge_2Te_6$. The Seebeck coefficients are $+65\,\mu V\,K^{-1}$ in case of $Tl_6Si_2Te_6$ and $+150\,\mu V\,K^{-1}$ in case of $Tl_6Ge_2Te_6$ at 300 K, and the electrical conductivities are 5.5 and $3\,\Omega^{-1}\,cm^{-1}$, respectively.

Keywords: Thallium; Silicon; Telluride; Crystal structure; Electronic structure; Semiconductor

1. Introduction

Thermoelectric materials are capable of converting heat into electricity and vice versa. Most state-of-the-art thermoelectrics are narrow gap semiconductors with heavy main group elements [1–4]. Within the last 10 years, several new and modified materials were found to outperform the commercially used ones [5–9]. Recent efforts into ternary main group thallium tellurides revealed materials with excellent thermoelectric properties because of their extremely low thermal conductivities. These include germanium and tin as the third element in Tl_2GeTe_5 and Tl_2SnTe_5 [10], antimony in $TlSbTe_2$ [11], and bismuth in Tl_9BiTe_6 [12] and $TlBiTe_2$ [13]. No example with silicon was known before the onset of our investigations. During the last years our group reported on new semiconducting low-valent tin chalcogenides [14] and polychalcogenides [15,16]. Here, we present our first results on low-valent thallium silicon and germanium tellurides, $Tl_6Si_2Te_6$ and $Tl_6Ge_2Te_6$.

*Corresponding author. Fax: +1 519 746 0435.
E-mail address: kleinke@uwaterloo.ca (H. Kleinke).

0022-4596/$ - see front matter © 2006 Elsevier Inc. All rights reserved.
doi:10.1016/j.jssc.2006.05.029

2. Experimental section

2.1. Synthesis and analysis

The elements were used directly as starting materials, stored in an argon-filled glove box (Tl: granules of lengths up to 5 mm, purity 99.999%, ALFA AESAR; Si: powder −100 mesh, 99.9%, ALFA AESAR; Ge: powder −100 mesh, 99.99%, ALDRICH; Te: powder, −325 mesh, 99.99%, ALFA AESAR). They were loaded in the stoichiometric 6:2:6 ratio into silica tubes, which were then sealed under vacuum. Subsequently, the tubes were heated in a resistance furnace to 800 °C within 24 h, and then cooled to 700 °C within 15 min. 800 °C was chosen to obtain a molten (hence homogeneous) mixture, which was then annealed at 700 °C for 200 h. Thereafter the furnace was switched off. The samples consisted mostly of black powder, together with few crystals of metallic luster. The materials are not air sensitive at room temperature over a period of a few weeks.

According to the X-ray diffractograms of the ground samples acquired with an INEL powder diffractometer

with a position-sensitive detector, both $Tl_6Si_2Te_6$ and $Tl_6Ge_2Te_6$ were obtained phase-pure. Moreover, the samples were analyzed by means of standardless energy dispersive spectroscopy (EDS, LEO 1530, with integrated EDAX Pegasus 1200) using an acceleration voltage of 21 kV. No heteroelements, e.g. stemming from the reaction container, were found in any case, and the distribution of the desired elements Tl, Te, and Si and Ge, respectively, appeared to be homogeneous in both samples, e.g. the crystals had the same stoichiometry as the rest of the samples.

2.2. Crystal structure determination

Since the structure of $Tl_6Ge_2Te_6$ was reported before [17], we investigated only $Tl_6Si_2Te_6$. The data collection of a block-shaped single crystal taken from the Si-containing sample was mounted onto a BRUKER Smart Apex CCD diffractometer utilizing Mo$K\alpha$ radiation. The data were collected by scans of 0.3° in ω in two blocks of 606 frames at $\phi = 0°$ and 120°, with exposure times of 60 s/frame. The data were corrected for Lorentz and polarization effects, and absorption corrections were based on fitting a function to the empirical transmission surface as sampled by multiple equivalent measurements [18], since the crystal faces could not be determined reliably for numerical absorption corrections.

The cell parameters indicated that $Tl_6Si_2Te_6$ might be isostructural with $Tl_6Ge_2Te_6$ (space group $P\bar{1}$). We therefore used the atomic positions of the $Tl_6Ge_2Te_6$ structure [17] as starting point for our structure refinement, carried out with the SHELXTL package [19]. The final refinement resulted in residual values of $R_1 = 4.8\%$ and w$R_2 = 7.1\%$. A tentative refinements of the occupancy factors of the Tl sites and the Si sites yielded values between 99% and 100.5%, i.e. insignificant deviations from full occupancies. Crystallographic details are listed in Table 1, and atomic positions and equivalent displacement parameters in Table 2. Further details of the crystal structure investigation can be obtained from the Fachinformationszentrum Karlsruhe, 76344 Eggenstein-Leopoldshafen, Germany (fax: +49 7247 808 666; e-mail: crysdata@fiz-karlsruhe.de) on quoting the depository number CSD-416310.

2.3. Electronic structure calculations

Self-consistent tight-binding *first principles* LMTO calculations (LMTO = linear muffin tin orbitals) using the atomic spheres approximation (ASA) [20,21] were performed. In the LMTO approach, the density functional theory is employed with the local density approximation (LDA) for the exchange correlation energy [22]. The following wavefunctions were used: for Tl 6*s*, 6*p*, and included via the downfolding technique [23] 6*d* and 5*f*; for Si 3*s*, 3*p*, and 3*d* (downfolded); for Ge 4*s*, 4*p*, and 4*d* (downfolded); and for Te 5*s*, 5*p*, 5*d* (downfolded) and 4*f* (downfolded). In both cases, 1796 independent *k* points of the first Brillouin zone were chosen via an improved tetrahedron method [24]. The densities of states (DOS) of the (not isostructural) K analogue, $K_6Si_2Te_6$, were computed for comparison [25]. We calculated the integrated crystal orbital Hamilton population (COHP) values (ICOHPs, COHP) [26,27] for the homonuclear cationic interactions of $Tl_6Si_2Te_6$, i.e. Tl–Tl and Si–Si. Also for comparison, we calculated the ICOHP's of elemental hexagonal thallium and elemental silicon as well as of the Tl–Tl interactions in Tl_5Te_3 [28].

Table 1
Crystallographic data of $Tl_6Si_2Te_6$

Empirical formula	$Tl_6Si_2Te_6$
Formula weight	2048.00 g mol^{-1}
Temperature	298(2) K
Wavelength	0.71073 Å
Crystal system	Triclinic
Space group	$P\bar{1}$ (no. 2)
a	9.4235(6) Å
b	9.6606(7) Å
c	10.3889(7) Å
α	89.158(2)°
β	96.544(2)°
γ	100.685(2)°
Volume	923.3(1) Å^3
No. of formula units, *Z*	2
Density (calculated)	7.37 g cm^{-3}
Absorption coefficient	61.6 mm^{-1}
F(000)	1652
Crystal size (mm)	0.084 × 0.044 × 0.026
Completeness to $\Theta = 30°$	95.7%
Reflections collected	7684
Independent reflections	5157 [*R*(int) = 0.052]
Refinement method	Full-matrix least-squares on F^2
Data	5157
Goodness-of-fit on F^2	0.994
R indices ($I > 2\sigma(I)$): R_1, wR_2	0.0477, 0.0713
Extinction coefficient	0.00132(4)
Largest diff. peak and hole	2.29 and −2.27 e Å^{-3}

Table 2
Atomic coordinates[a] and equivalent displacement parameters[b] of $Tl_6Si_2Te_6$

Atom	*x*	*y*	*z*	U_{eq}/Å^2
Tl1	0.36141(7)	0.22161(8)	0.91569(7)	0.0436(2)
Tl2	0.09809(6)	0.43460(7)	0.65067(6)	0.0360(2)
Tl3	0.09350(8)	0.03967(8)	0.35334(7)	0.0508(2)
Tl4	0.48659(7)	0.38223(7)	0.35425(7)	0.0412(2)
Tl5	0.68253(6)	0.28855(7)	0.76046(6)	0.0369(2)
Tl6	0.80222(7)	0.14560(7)	0.15303(7)	0.0440(2)
Si1	0.0885(4)	0.4282(4)	0.0138(4)	0.0192(8)
Si2	0.576(4)	0.0168(4)	0.4172(4)	0.0185(8)
Te1	0.4206(1)	0.0664(1)	0.21571(9)	0.0281(2)
Te2	0.3163(1)	0.2013(1)	0.59206(9)	0.0267(2)
Te3	−0.0017(1)	0.2039(1)	0.8919(1)	0.0284(2)
Te4	0.69047(9)	0.4415(1)	0.0791(1)	0.0272(2)
Te5	0.12824(9)	0.3804(1)	0.25209(9)	0.0265(2)
Te6	0.77787(9)	0.2240(1)	0.4730(1)	0.0260(2)

[a] All atoms are on Wyckoff site 2*i*.
[b] U_{eq} is defined as one-third of the trace of the orthogonalized U_{ij} tensor.

2.4. Physical property measurements

Since single crystals could not be prepared with sufficient sizes for property measurements, we (cold-)pressed parts of the two ground phase-pure samples into two bar-shaped pellets of the dimensions $6 \times 1 \times 1\,mm^3$. The densities achieved were about 80% of the hypothetical densities as determined via X-ray diffraction. Seebeck coefficients (thermopower, S) were determined with a commercial thermopower system (MMR Technologies). Electrical conductivities (σ) were measured by determining the voltage drops ΔV over a distance of 2 mm under dynamic vacuum employing a self-made device with a helium compressor. The resistances (R) were calculated from the voltage drops using Ohm's law, i.e. $R = \Delta V/I$, with $I =$ current. We calculated $\sigma(T)$ after measuring the lengths between the contacts, L, according to $\sigma = L/(AR)$, with the area $A = 1\,mm \times 1\,mm$.

3. Results and discussion

3.1. Crystal structures

$Tl_6Si_2Te_6$ is the first thallium silicon telluride, while two selenides are known, Tl_4SiSe_4 and Tl_2SiSe_3 [29]. The crystal structure of $Tl_6Si_2Te_6$ is shown in Fig. 1, which omits the Tl–Te bonds for clarity. Besides the numerous Tl–Tl contacts between 3.54 and 3.99 Å (dashed lines in Fig. 1, listed in Table 3), the most striking structural features are the molecular Si_2Te_6 units, which are interconnected via Tl–Te interactions. The Si_2Te_6 units comprise both Si sites and all six Te sites of the $Tl_6Si_2Te_6$ structure.

Both crystallographically independent Si_2Te_6 units are depicted in Fig. 2. They are topologically equivalent, with each Si atom pseudo-tetrahedrally coordinated by one Si and three Te atoms. In both cases, an inversion center is located in the center of the Si–Si bond. The two Si–Si bond lengths, 2.34 and 2.35 Å, are typical for Si–Si single bonds, as also present in the element adopting the diamond structure, where four Si–Si single bonds of 2.35 Å per Si atom exist. The Si–Te bonds of approximately 2.5 Å compare well with the sum of the covalent single bond radii $r_{Si} + r_{Te} = 1.17\,Å + 1.37\,Å = 2.54\,Å$ [30].

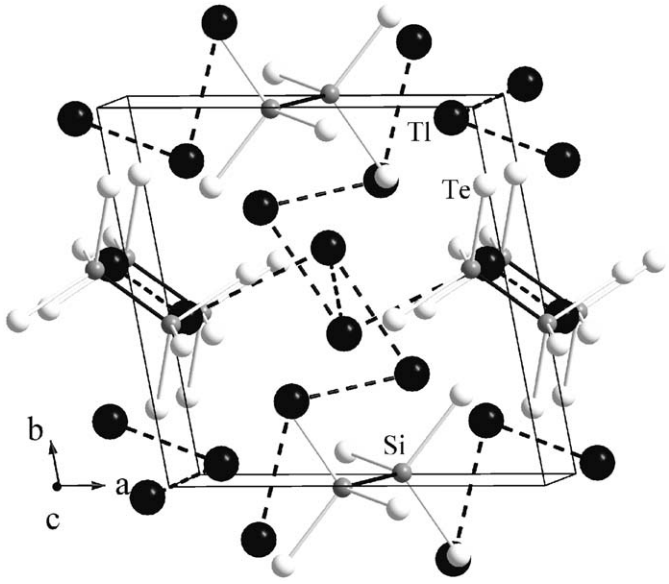

Fig. 1. Crystal structure of $Tl_6Si_2Te_6$.

Table 3
Selected interatomic distances (Å) of $Tl_6Si_2Te_6$

Tl1–Te2	3.345(1)	Tl2–Te5	3.274(1)
Tl1–Te3	3.375(1)	Tl2–Te4	3.350(1)
Tl1–Te4	3.381(1)	Tl2–Te2	3.424(1)
Tl1–Te1	3.471(1)	Tl2–Te3	3.425(1)
Tl1–Tl5	3.5400(9)	Tl2–Tl2	3.774(1)
Tl1–Tl6	3.642(1)	Tl2–Te6	3.562(1)
Tl1–Te4	3.671(1)	Tl2–Te6	3.636(1)
Tl3–Te2	3.272(1)	Tl4–Te1	3.315(1)
Tl3–Te5	3.410(1)	Tl4–Te2	3.387(1)
Tl3–Te3	3.420(1)	Tl4–Te5	3.419(1)
Tl3–Te6	3.424(1)	Tl4–Te6	3.482(1)
Tl3–Te1	3.509(1)	Tl4–Te4	3.604(1)
Tl3–Tl6	3.548(1)	Tl4–Tl4	3.772(2)
Tl3–Tl3	3.692(2)		
		Tl6–Te4	3.277(1)
Tl5–Te6	3.315(1)	Tl6–Te3	3.435(1)
Tl5–Te3	3.366(1)	Tl6–Te6	3.462(1)
Tl5–Te5	3.369(1)	Tl6–Te5	3.522(1)
Tl5–Te1	3.340(1)	Tl6–Tl3	3.548(1)
Tl5–Te4	3.632(1)	Tl6–Tl1	3.642(1)
Tl5–Te2	3.643(1)	Tl6–Te4	3.666(1)
Si1–Si1	2.351(7)	Si2–Si2	2.338(7)
Si1–Te3	2.485(4)	Si2–Te1	2.506(4)
Si1–Te4	2.510(4)	Si2–Te2	2.512(4)
Si1–Te5	2.511(4)	Si2–Te6	2.518(4)

One Si–Si bond per Si atom is indicative of tri-valent Si, as found in $Na_4Si_2Te_5$ (2.37 Å) [28], $Na_6Si_2Te_6$ (2.35 Å) [31], and $K_6Si_2Te_6$ (2.41 Å) [25]. In these examples, the valence-electrons may be readily assigned; as there are no bonding Te–Te contacts, and the alkaline metals are in their common +I oxidation state, silicon is in its +III state in all three cases, $(Na^I)_4(Si^{III})_2(Te^{2-})_5$, $(Na^I)_6(Si^{III})_2(Te^{2-})_6$, and $(K^I)_6(Si^{III})_2(Te^{2-})_6$. Correspondingly, we postulate the same assignments in $Tl_6Si_2Te_6$, resulting in $(Tl^I)_6(Si^{III})_2(Te^{2-})_6$. Similarly, the Ge–Ge bonds of $Tl_6Ge_2Te_6$ (2.45 and 2.46 Å) are classified as single bonds, as in $K_6(Ge^{III})_2Te_6$ (2.49 Å) [32] and $Ba_2(Ge^{III})_2Te_5$ (2.47 Å) [33], leading to the analogous formulation $(Tl^I)_6(Ge^{III})_2(Te^{2-})_6$.

In many structures Tl^I may replace K^I; however, $Tl_6Si_2Te_6$ and $K_6Si_2Te_6$ form different structures with comparable $(Si^{III})_2(Te^{2-})_6^{6-}$ units ($K_6Ge_2Te_6$ occurs in another type, with topologically equivalent $Ge_2Te_6^{6-}$ units). This fact is reflected in numerous Tl–Tl contacts in $Tl_6Si_2Te_6$ as short as 3.54 Å, whereas the shortest K–K distance of $K_6Si_2Te_6$ is 3.83 Å. The corresponding values for the Ge tellurides are 3.55 Å (Tl–Tl in $Tl_6Ge_2Te_6$) and 3.86 Å (K–K in $K_6Ge_2Te_6$) While the K^I–K^I interactions

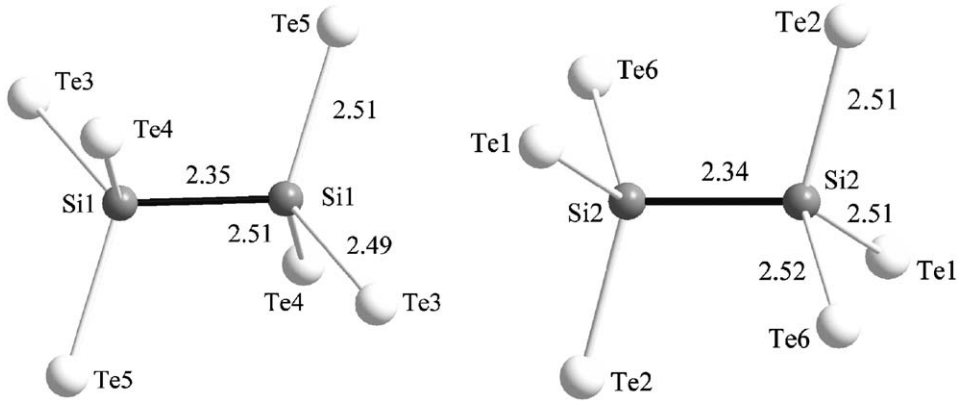

Fig. 2. The two symmetry-independent $Si_2Te_6^{6-}$ units of $Tl_6Si_2Te_6$.

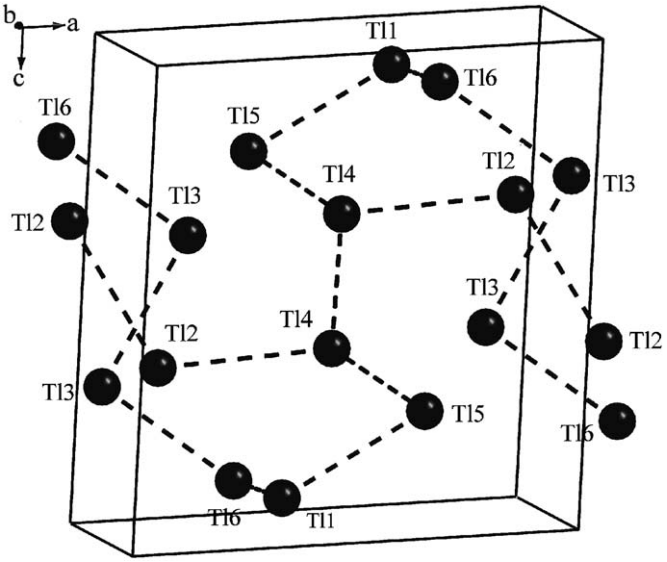

Fig. 3. The two-dimensional network of Tl atoms of $Tl_6Si_2Te_6$.

must be repulsive, because of the s^0 configuration of K^I, there is a strong tendency of Tl^I to participate in (weakly) bonding Tl–Tl interactions [34,35] that can be as short as 3.37 Å (observed in Tl_2Te [36]). The Tl atom network extends itself infinitely parallel to the *a*, *b* plane in $Tl_6Si_2Te_6$ and $Tl_6Ge_2Te_6$, and may thus be regarded as a wide puckered layer (Fig. 3).

The shortest Tl–Tl contact of 3.54 Å in $Tl_6Si_2Te_6$ is comparable to the shortest contacts in Tl_5Te_3 (3.46–3.50 Å), which also form a two-dimensional net. These distances are of the same order as the Tl–Te distances in $Tl_6Si_2Te_6$, ranging from 3.28 to 3.67 Å ($Tl_6Ge_2Te_6$: 3.27–3.58 Å). The next longest Tl–Te distances are 4.05 Å in $Tl_6Si_2Te_6$ and 3.97 Å in $Tl_6Ge_2Te_6$. These Tl–Te distances are inconspicuous, comparing nicely to the Tl–Te distances of the 6-coordinated Tl atom in $(Tl^I)_2Te$ (3.30–3.42 Å) [36]. The six Tl sites of $Tl_6Si_2Te_6$ exhibit between five and six neighboring Te atoms at distances <3.7 Å, whereas each K site of $K_6Si_2Te_6$ is coordinated by six Te atoms at distances between 3.45 and 3.81 Å. The Tl–Te polyhedra of $Tl_6Si_2Te_6$ and $Tl_6Ge_2Te_6$ are in part extremely irregular, allowing for close contacts between the Tl atoms. This is most evident for the Tl1, Tl3, and Tl4 sites (Fig. 4). One might postulate an inert pair effect of the Tl–6*s* orbital, but we will show in the "Electronic structure" chapter that the *s* orbital participates in Tl–Tl bonding. The extremely irregular Tl–Te polyhedra combined with the arrangement of the Tl atoms require the adoption of the rather rare triclinic crystal system for $Tl_6Si_2Te_6$.

3.2. Electronic structures

The computed DOS of $Tl_6Si_2Te_6$ and $Tl_6Ge_2Te_6$ are compared in Fig. 5, with the Fermi level, E_F, arbitrarily placed at 0 eV. As expected for related isostructural and isovalent materials, there are strong resemblances. Outside of the chosen energy window are the filled Te–5*s* states, occurring between -11 and -12.5 eV. Lowest in energy within the Fig. 5 are the *s* states of the group 14 elements, E = Si, Ge, located below -8 eV. The peak above that is comprised of Te-centered states exhibiting *E*–*s*–Te–*p* bonding character, followed by the Tl–6*s* states (highlighted via dashed lines). The latter overlap with the Si–*s*–Te–*p* peak just below -6 eV, but not with the Ge–*s*–Te–*p* peak around -7 eV. The large valence band, extended between -4 eV and E_F, is predominated by Te–5*p* states, which have overall bonding Tl–Te and *E*–Te character. The Tl–Te interactions are weakened by the presence of antibonding states just below E_F.

The conduction band comprises Tl–*p* and *E*–*p* contributions, of mostly antibonding Tl–Te and *E*–Te character. A band gap of 0.9 eV in $Tl_6Si_2Te_6$ and of 0.5 eV in $Tl_6Ge_2Te_6$ separates the valence and conduction band. Hence, both tellurides are narrow gap semiconductors, consistent with their black appearance. That the gap is smaller in case of the Ge telluride is a consequence of the higher covalent character of the Ge–Te interactions. We computed the gap of the K analogue, $K_6Si_2Te_6$, to be 1.8 eV. The large difference results from the higher ionicity of the latter, since K is much less electronegative than Tl,

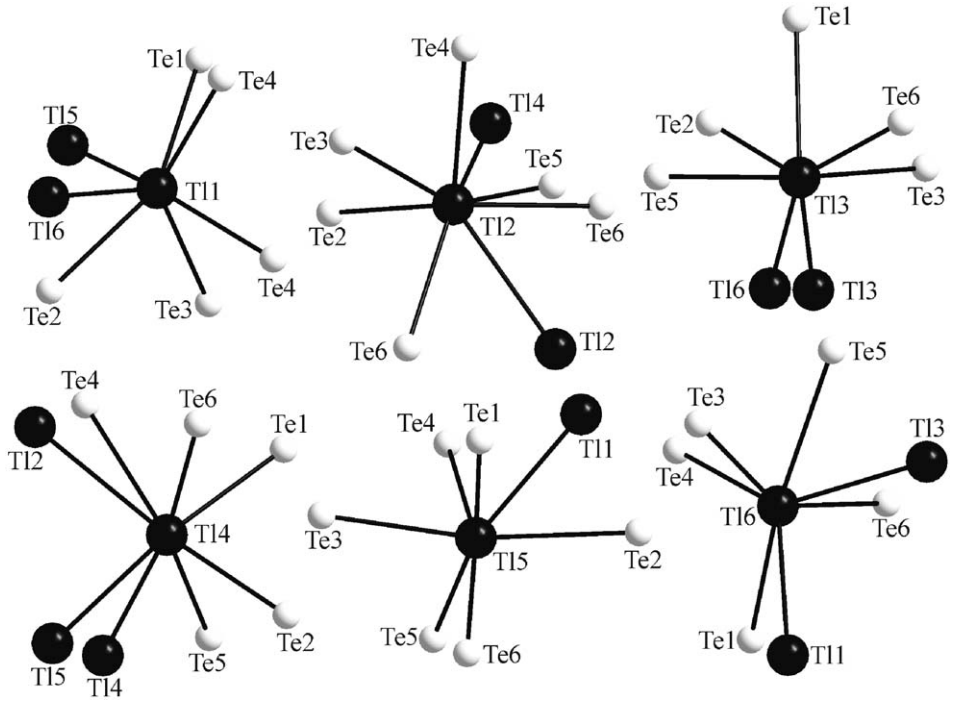

Fig. 4. The first coordination spheres of the six independent Tl sites of $Tl_6Si_2Te_6$.

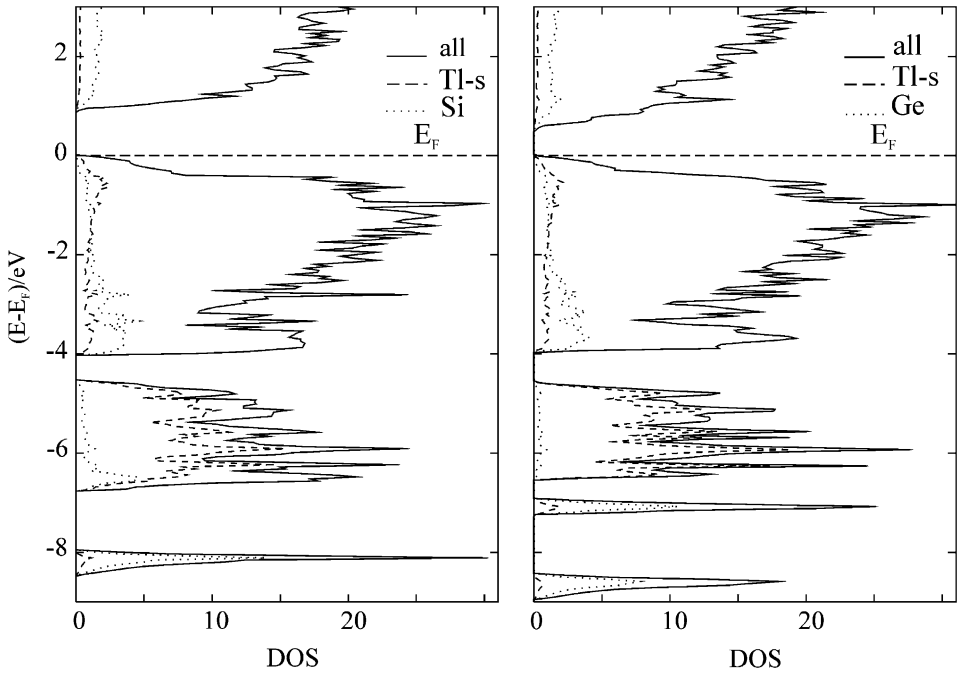

Fig. 5. Densities of States of $Tl_6Si_2Te_6$ (left) and $Tl_6Ge_2Te_6$ (right).

e.g. Pauling' electronegativities are 0.82 for K and 2.04 for Tl (and 2.10 for Te).

The COHP curves of the homonuclear Tl–Tl and *E–E* interactions, cumulated over the whole unit cell of $Tl_6Si_2Te_6$, are shown in Fig. 6. The Si–Si COHP curve, formed by the two bonds of 2.34 and 2.35 Å, is dominated by the strong *s–s* interaction located in a sharp peak at −8 eV. This is consistent with Si^{III}, and one filled *s–s* bonding and one empty *s–s* antibonding orbital per Si_2 unit, the latter located 5 eV above E_F (outside the energy window chosen). The small contributions between −4 eV and E_F are a consequence of the covalent mixing with the Te states. Both bonds are comparably strong, with calculated ICOHP values of −2.70 and −2.83 eV per bond. For comparison, we calculated the ICOHP for the Si–Si bond in elemental silicon to be −3.15 eV.

Eight Tl–Tl interactions were added up to give the Tl–Tl COHP curve shown in the right part of Fig. 6. For a graphical comparison with the Si–Si interaction, the different COHP scale (between −3 and 3, compared to −20 to +20 per cell) must be noted. As for the Si–Si interactions, the strongest contributions come from the *s* orbitals, which a comparison of the projection of the Tl–*s* states onto the DOS shows, located between −4.5 and −7 eV. However, here both bonding and antibonding states are filled, consistent with Tl^{I}. The integration over the whole COHP curve reveals that the bonding contributions clearly outweigh the antibonding, resulting in ICOHP values between −0.26 eV for the Tl1–Tl5 interaction (3.54 Å) and −0.06 eV for the Tl2–Tl4 contact (3.99 Å). Stronger bonds were found in elemental thallium (hexagonal closed packed modification), namely 6×0.41 eV (3.41 Å) and 6×0.48 eV (3.46 Å). The Tl–Tl interactions in the binary telluride, Tl_5Te_3, exhibit comparable values, with the largest being −0.19 eV for the 3.50 Å contact.

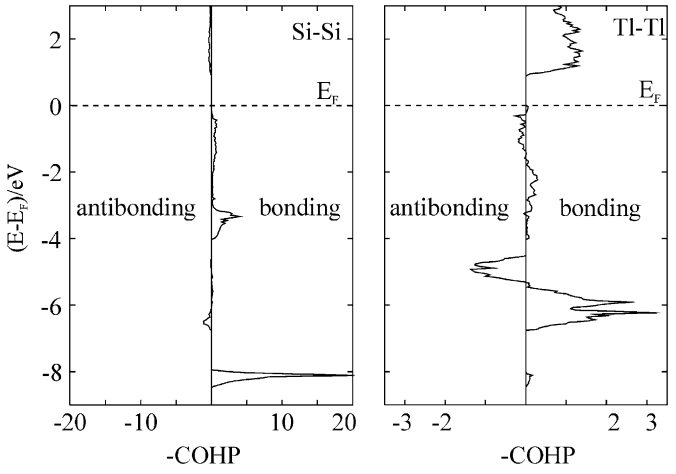

Fig. 6. Crystal orbital Hamilton population curves of the homonuclear Si–Si (left) and Tl–Tl (right) interactions of $Tl_6Si_2Te_6$.

3.3. Physical properties

The measured Seebeck coefficients (S) and electrical conductivities (σ) of $Tl_6Si_2Te_6$ and $Tl_6Ge_2Te_6$ are shown in Fig. 7. Between 300 and 460 K, the Seebeck coefficients increase with increasing temperatures in both cases, with values from $S = +65$ to $+95\,\mu V\,K^{-1}$ for $Tl_6Si_2Te_6$ and $+150$ to $+210\,\mu V\,K^{-1}$ for $Tl_6Ge_2Te_6$. The electrical conductivities of $Tl_6Si_2Te_6$ decrease slowly with increasing temperatures, namely from $\sigma = 6.7\,\Omega^{-1}\,cm^{-1}$ at 180 K to $5.2\,\Omega^{-1}\,cm^{-1}$ at 295 K, corresponding to a negative slope. On the other hand, the electrical conductivities of $Tl_6Ge_2Te_6$ follow the opposite trend: they increase from $2.7\,\Omega^{-1}\,cm^{-1}$ at 180 K to $3.0\,\Omega^{-1}\,cm^{-1}$ at 295 K (a positive slope).

The observations of flat conductivity curves and moderate Seebeck coefficients are indicative with extrinsic semiconductors, while the positive Seebeck coefficients reveal that the *p*-type carriers dominate. The negative slope of the conductivity of $Tl_6Si_2Te_6$ points towards a large number of charge carriers being present, possibly caused by small defects in the crystal structure not detected by the X-ray studies. This also explains the rather high conductivities and small Seebeck coefficients for a material with a computed gap of 0.9 eV (co-existence of positive and negative charge carriers). On the other hand, the positive albeit flat conductivity slope of $Tl_6Ge_2Te_6$ is likely caused by a smaller number of extrinsic charge carriers, consistent with its higher Seebeck coefficients. We refrained from measuring the properties of $K_6Si_2Te_6$ because of its air sensitivity [25] and its large computed gap of 1.8 eV.

Overall the electrical conductivities are relatively high for materials with calculated band gaps between 0.5 and 0.9 eV, in particular when considering that the calculation method usually underestimates the band gap [37]. In addition to the above-mentioned defects, high mobility of the charge carriers caused by the high covalent bonding character as well as the extended Tl atom network

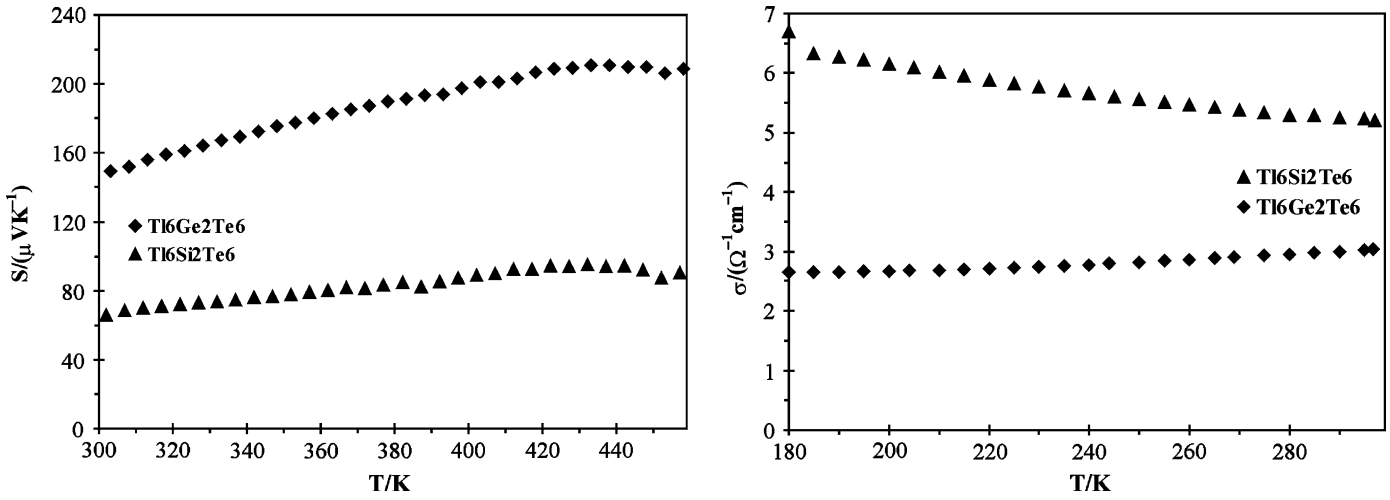

Fig. 7. Seebeck coefficients (left) and electrical conductivities (right) of $Tl_6Si_2Te_6$ (triangles) and $Tl_6Ge_2Te_6$ (squares).

contributes to the conductivities. However, significantly higher electrical conductivities are required for the thermoelectric energy conversion, while the measured Seebeck coefficients are acceptable. E.g., $TlSbTe_2$ exhibits $\sigma = 1000\,\Omega\,cm^{-1}$ and $S = +80\,\mu V\,K^{-1}$ [11], and $AgPb_{18}SbTe_{20}$ $\sigma = 1820\,\Omega\,cm^{-1}$ and $S = -135\,\mu V\,K^{-1}$ at room temperature [8], the latter being a superior high-temperature thermoelectric material. It remains to be seen in how far the physical properties of $Tl_6Si_2Te_6$ and $Tl_6Ge_2Te_6$ can be optimized by (a) hot-pressing (hence decreasing the grain boundary effect) and (b) systematic doping (eliminating the presence of both charge carrier types, and increasing the concentration of the *p*-type carriers).

4. Conclusions

A new telluride, $Tl_6Si_2Te_6$, was prepared and characterized. It is the first one found in the Tl–Si–Te system. Its structure, isostructural with $Tl_6Ge_2Te_6$, is composed of $(Si^{III})_2Te_6^{6-}$ units with a central Si–Si bond, irregular Tl^ITe_5 and Tl^ITe_6 polyhedra, and a two-dimensional Tl atom network comprising weak albeit significantly bonding Tl–Tl interactions. $Tl_6Si_2Te_6$ and $Tl_6Ge_2Te_6$ were calculated to be small band gap semiconductors. Physical property measurements revealed room temperature conductivities of several $\Omega\,cm^{-1}$ and Seebeck coefficients of $+65\,\mu V\,K^{-1}$ for $Tl_6Si_2Te_6$ and $+150\,\mu V\,K^{-1}$ for $Tl_6Ge_2Te_6$.

Acknowledgments

Financial support from NSERC, CFI, OIT (Ontario Distinguished Researcher Award for H.K.), MMO and the Canada Research Chair program (CRC for H.K.) is appreciated.

References

[1] T.M. Tritt, Science 272 (1995) 1276–1277.
[2] D.M. Rowe, CRC Handbook of Thermoelectrics, CRC Press, Boca Raton, FL, 1995.
[3] F.J. DiSalvo, Science 285 (1999) 703–706.
[4] T.M. Tritt, Science 283 (1999) 804–805.
[5] B.C. Sales, D. Mandrus, R.K. Williams, Science 272 (1996) 1325–1328.
[6] D.-Y. Chung, T. Hogan, P. Brazis, M. Rocci-Lane, C. Kannewurf, M. Bastea, C. Uher, M.G. Kanatzidis, Science 287 (2000) 1024–1027.
[7] R. Venkatasubramanian, E. Slivola, T. Colpitts, B. O'Quinn, Nature 413 (2001) 597–602.
[8] K.F. Hsu, S. Loo, F. Guo, W. Chen, J.S. Dyck, C. Uher, T. Hogan, E.K. Polychroniadis, M.G. Kanatzidis, Science 303 (2004) 818–821.
[9] D.-Y. Chung, T.P. Hogan, M. Rocci-Lane, P. Brazis, J.R. Ireland, C.R. Kannewurf, M. Bastea, C. Uher, M.G. Kanatzidis, J. Am. Chem. Soc. 126 (2004) 6414–6428.
[10] J.W. Sharp, B.C. Sales, D.G. Mandrus, B.C. Chakoumakos, Appl. Phys. Lett. 74 (1999) 3794–3796.
[11] K. Kurosaki, H. Uneda, H. Muta, S. Yamanaka, J. Alloys Compd. 376 (2004) 43–48.
[12] B. Wolfing, C. Kloc, J. Teubner, E. Bucher, Phys. Rev. Lett. 86 (2001) 4350–4353.
[13] K. Kurosaki, A. Kosuga, S. Yamanaka, J. Alloys Compd. 351 (2003) 279–282.
[14] A. Assoud, N. Soheilnia, H. Kleinke, Chem. Mater. 16 (2004) 2215–2221.
[15] A. Assoud, S. Derakhshan, N. Soheilnia, H. Kleinke, Chem. Mater. 16 (2004) 4193–4198.
[16] A. Assoud, N. Soheilnia, H. Kleinke, J. Solid State Chem. 178 (2005) 1087–1093.
[17] G. Eulenberger, J. Solid State Chem. 55 (1984) 306–313.
[18] SAINT, Version 4 ed., Siemens Analytical X-ray Instruments Inc., Madison, WI, 1995.
[19] G.M. Sheldrick, SHELXTL, Version 5.12 ed., Siemens Analytical X-ray Systems, Madison, WI, 1995.
[20] O.K. Andersen, Phys. Rev. B 12 (1975) 3060–3083.
[21] H.L. Skriver, The LMTO Method, Springer, Berlin, Germany, 1984.
[22] L. Hedin, B.I. Lundqvist, J. Phys. C 4 (1971) 2064–2083.
[23] W.R.L. Lambrecht, O.K. Andersen, Phys. Rev. B 34 (1986) 2439–2449.
[24] P.E. Blöchl, O. Jepsen, O.K. Andersen, Phys. Rev. B 49 (1994) 16223–16233.
[25] G. Dittmar, Angew. Chem. Int. Ed. Engl. 16 (1977) 554.
[26] R. Dronskowski, P.E. Blöchl, J. Phys. Chem. 97 (1993) 8617–8624.
[27] G.A. Landrum, R. Dronskowski, Angew. Chem. Int. Ed. 39 (2000) 1560–1585.
[28] B. Eisenmann, H. Schwerer, H. Schäfer, Rev. Chim. Min. 20 (1983) 78–87.
[29] G. Eulenberger, Monatsh. Chem. 113 (1982) 859–867.
[30] L. Pauling, The Nature of the Chemical Bond, third ed, Cornell University Press, Ithaca, NY, 1948.
[31] B. Eisenmann, H. Schwerer, H. Schäfer, Z. Naturforsch. B 36 (1981) 1538–1541.
[32] G. Dittmar, Z. Anorg. Allg. Chem. 453 (1979) 68–78.
[33] C. Brinkmann, B. Eisenmann, H. Schäfer, Z. Anorg. Allg. Chem. 517 (1984) 143–148.
[34] C. Janiak, R. Hoffmann, J. Am. Chem. Soc. 112 (1990) 5924–5946.
[35] P. Pyykkö, Chem. Rev. 97 (1997) 597–636.
[36] R. Cerny, J.M. Joubert, Y. Filinchuk, Y. Feutelais, Acta Crystallogr. C 58 (2002) i63–i65.
[37] H. Yanagi, S.-I. Inoue, K. Ueda, H. Kawazoe, J. Appl. Phys. 88 (2000) 4159–4163.